# Design optimization of a direct-drive PMSG considering the torque-speed profile Application for Offshore wind energy

***Abstract* – This paper presents an optimal design methodology taking speed and torque profiles into account for permanent magnet synchronous generators (PMSGs). This method, based on the d-q axis equivalent circuit model, allows to optimize both the time-dependent control parameters and the design with a reduced computation time. The case of a 10-MW direct-driven Permanent Magnet Generator for an Offshore wind turbine has been chosen to illustrate this method. The design objective is to minimize the masse as well as the average electric losses over all working points. Thermal and magnetic models are validated by a finite element analysis (FEA).**

***Index Terms*—Wind speed profile, Loss minimizing control, PMSG, Design optimization.**

## I. NOMENCLATURE

$v_d, v_q$ : d-and q- axis terminal voltages [V]
$i_d, i_q$ : d- and q- axis currents [A]
$e_0$ : back electromotive force [V]
$\mathcal{R}_c$ : armature resistance [Ω]
$\mathcal{R}_\mu$ : iron loss resistance [Ω]
$X$ : synchronous reactance [Ω]
$P_c$ : copper losses [W]
$P_{mg}$ : iron losses [W]
$k_{ad}$ : additional iron loss coefficient
$k_{ec}$ : eddy currents specific loss coefficient
$k_h$ : hysteresis specific loss coefficient
$k_f$ : slot fill factor
$k_t$ : tooth opening to the slot pitch ratio
$k_L$ : coefficient for correcting the active length
$L$ : active length [m]
$\tau_{LR}$ : length to outer stator radius ratio
$R$ : outer stator radius [m]
$R_s$ : inner stator radius [m]
$R_r$ : outer rotor radius [m]
$r_s$ : reduced inner stator radius
$R_w$ : outer winding radius [m]
$r_w$ : reduced outer winding radius
$w_{ag}$ : air-gap thickness [m]
$w_{PM}$ : permanent magnet height[m]
$b_{PM}$ : permanent magnet width [m]
$n_s$ : number of turns per phase per pole
$p$ : number of pole pairs
$q$ : number of phase
$\sigma_c$ : electric conductivity [$S^{-1}$]
$\Omega_m$ : machine mechanical angular velocity [rad/s]
$\theta_{max}$ : maximal permissible temperature [°C]
$\theta_w$ : maximal winding temperature [°C]
$\theta_{amb}$ : ambient temperature [°C]
$h_{eq}$ : heat transfer coefficient [W/m²K]
$\rho_c$ : copper density [kg/ $m^3$]
$\rho_{Fe}$ : steel density [kg/ $m^3$]
$\rho_{PM}$ : permanent magnet density [kg/ $m^3$]
$C_{pc}$ : specific heat capacity of copper [J/Kg/K]
$C_{pFe}$ : specific heat capacity of steel [J/Kg/K]

## II. INTRODUCTION

OFFSHORE wind generation has taken an increasingly important place in the European wind power development in the last recent years. It presents a high availability, stable wind speed and less environmental constraints. In order to reduce the energy cost, increasing the turbine power is a strong trend. However, it leads to increase active and structural masses which are limited by technology, transport and installation. Therefore, maximizing the power density is a crucial criterion in the design process.

In that case, variable-speed wind turbines with pitch control are used [1] to optimize the turbine output power. Generally, the dynamic behavior is not taken into account in the design process. In most cases, the generator is designed for the rated power [2], [3] only. Such a method can lead to oversize the generator particularly if the permanent thermal regime is not reached. To minimize energy losses, all working points must be considered. One of the most important issues, in a design process which consider several hundreds of working points, is that, in addition to optimizing the dimension parameters, it must also optimize the time-dependent control parameters. Therefore, that leads to a huge computation time. In order to overcome this problem, the present solutions replace all working points by some representative ones [4]. However, such an approach does not allow to consider an optimal control strategy as well as the thermal transient phenomenon.

The aim of this paper is to present an optimal design methodology which considers all working points of the wind generator without increasing the computation time. The proposed method allows to optimize simultaneously the geometry as well as the control parameters of each working point. In addition, it allows also to reduce the constraint on the power electronics converter [5]. In this paper, the case of a 10-MW direct-drive PMSG with nine phases, taking a real wind speed profile into account, has been investigated. Considering the crucial constraints presented above, the purpose of our

This work was carried out within the framework of the WEAMEC, West Atlantic Marine Energy Community, and with funding from the Pays de la Loire Region.

work is to minimize both the mass and the average losses considering a monthly working cycle.

The paper is organized as follows. At first, the principle of the optimal design methodology will be detailed. Then, the different models and constraints used will be given. Next, the results of the selected optimum machine with its optimum geometry and optimum time-dependent currents will be presented and discussed. The last part of the paper is dedicated to validate, by the use of a 2D Finite Element Analysis (FEA), the analytical model used.

## III. Optimal design methodology

The presented methodology is based on the d-q axis equivalent circuit model taking iron losses into account via the iron loss resistance $R_\mu(t)$ (see Fig. 1). The optimization parameters can be categorized into three groups as below:

- The time-dependent control variables are the d-q axis currents $i_{oq}(t)$ and $i_{od}(t)$. They will be analytically expressed to minimize the sum of iron and copper power losses for each working points.
- The rotor variable $B_{fm}$, magnitude of the air-gap flux density represented in the circuit via the electromotive force $e_0(t)$. It will be optimized analytically to minimize the energy losses for the considered cycle. Note that the magnets are sized afterwards, from $B_{fm\,opt}$.
- The stator geometry variables are $R, r_s, r_w$ and $p$ (see Fig. 2) which are in the reactance ($X$) and resistances ($\mathcal{R}_c, \mathcal{R}_\mu$) expressions (see Fig.1). They will be optimized by the use of a genetic algorithm to minimize the average losses of all working points.

The optimization approach described here is based on the principle presented in [5]. At first, both the optimal currents ($i_{oq\,opt}(t), i_{od\,opt}(t)$) and the optimal magnitude of the air-gap flux density of the permanent magnets ($B_{fm\,opt}$) will be predetermined analytically as a function of the geometric parameters, the power and speed profiles. These results, in a second step, allow to express analytically the average losses over the working cycle as a function of the geometric parameters only. In the final step, a genetic algorithm will be used to find the optimal design parameters.

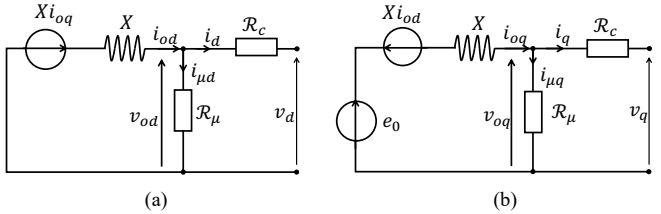


*Fig. 1. (a) d-axis equivalent circuit of an PMSG; (b) q-axis equivalent circuit of an PMSG*

### A. Basic equations

In this article, due to low speed and torque variations, the terms in $d/dt$ will be neglected. Then, the main equations such as the d-q axis stator voltages ($v_{od}(t), v_{oq}(t)$) and the electromagnetic power ($P_{em}(t)$) can be expressed as:

$$v_{od}(t) = X(t) i_{oq}(t) \tag{1}$$

$$v_{oq}(t) = -X(t) i_{od}(t) + e_0(t) \tag{2}$$

$$P_{em}(t) = i_{oq}(t) e_0(t) \tag{3}$$

The copper losses $P_c(t)$ can be calculated as:

$$P_c(t) = \mathcal{R}_c\left(i_d^2(t) + i_q^2(t)\right) \tag{4}$$

Where:

$$i_d(t) = i_{od}(t) - i_{\mu d}(t) = i_{od}(t) - \frac{v_{od}(t)}{\mathcal{R}_\mu(t)} \tag{5}$$

$$i_q(t) = i_{oq}(t) - i_{\mu q}(t) = i_{oq}(t) - \frac{v_{oq}(t)}{\mathcal{R}_\mu(t)} \tag{6}$$

From (1), (2), (4), (5) and (6), the copper losses can be expressed as follows:

$$P_c(t) = i_{od}^2(t)\left(\mathcal{R}_c + \mathcal{R}_c\left(\frac{X(t)}{\mathcal{R}_\mu(t)}\right)^2\right) + \cdots \tag{7}$$

$$\ldots + i_{oq}^2(t)\left(\mathcal{R}_c + \mathcal{R}_c\left(\frac{X(t)}{\mathcal{R}_\mu(t)}\right)^2\right) + \cdots$$

$$\ldots - i_{od}(t)\frac{2e_0(t)\mathcal{R}_c X(t)}{\mathcal{R}_\mu^2(t)} + \cdots$$

$$\ldots - i_{oq}(t)\frac{2e_0(t)R_c}{\mathcal{R}_\mu(t)} + \frac{\mathcal{R}_c e_0^2(t)}{\mathcal{R}_\mu^2(t)}$$

The iron losses are expressed as:

$$P_{mg}(t) = \frac{v_{od}^2(t) + v_{oq}^2(t)}{\mathcal{R}_\mu(t)} \tag{8}$$

From (1), (2) and (8), it is possible to write:

$$P_{mg}(t) = i_{oq}^2(t)\frac{X^2(t)}{\mathcal{R}_\mu(t)} + i_{od}^2(t)\frac{X^2(t)}{\mathcal{R}_\mu(t)} + \cdots \tag{9}$$

$$\ldots - i_{od}(t)\frac{2X(t)e_0(t)}{\mathcal{R}_\mu(t)} + \frac{e_0^2(t)}{\mathcal{R}_\mu(t)}$$

### B. Analytical expression of the optimal currents

The optimal currents allows the generator to satisfy the requested power $P_{em}(t)$ and speed $\Omega_m(t)$ with minimal losses. For the PMSG, the q-axis current $i_{oq\,opt}(t)$ is directly imposed by the electromagnetic power $P_{em}(t)$ according to (10) such as:

$$i_{oq\,opt}(t) = -\frac{P_{em}(t)}{e_0(t)} \tag{10}$$

Then, from (7), (8) and (10), the sum of the iron and copper losses, for a given geometry, can be expressed as:

$$P_t(t) = P_c(t) + P_{mg}(t) = i_{od}^2(t)A(t) + \cdots \tag{11}$$

$$\ldots - 2e_0(t)X(t)B(t)i_{od}(t) + \left(-\frac{P_{em}(t)}{e_0(t)}\right)^2 A(t) + \cdots$$

$$\ldots + \frac{2P_{em}(t)\mathcal{R}_c}{\mathcal{R}_\mu(t)} + e_0^2(t)B(t)$$

Where the terms $A(t)$ and $B(t)$ depend on the resistances and the reactance as following:

$$A(t) = \mathcal{R}_c + \mathcal{R}_c\left(\frac{X(t)}{\mathcal{R}_\mu(t)}\right)^2 + \frac{X^2(t)}{\mathcal{R}_\mu(t)} \quad (12)$$

$$B(t) = \frac{\mathcal{R}_c + \mathcal{R}_\mu(t)}{\mathcal{R}_\mu^2(t)} \quad (13)$$

From (11), it can be shown that the total losses are minimized with:

$$i_{od\ opt}(t) = \frac{e_0(t)X(t)B(t)}{A(t)} \quad (14)$$

And:

$$P_{t_{opt}}(t) = \left(B(t) - \frac{\left(X(t)B(t)\right)^2}{A(t)}\right)e_0^2(t) + \cdots \quad (15)$$

$$\ldots + \frac{A(t)P_{em}^2(t)}{e_0^2(t)} + \frac{2P_{em}(t)\mathcal{R}_c}{\mathcal{R}_\mu(t)}$$

### C. *Analytical expression of $B_{fm\ opt}$*

The magnitude of the magnetic flux density $B_{fm}$ produced by the magnets in the air-gap is constant, whatever the working point. This parameter is then optimized by the minimization of the average losses over the cycle. By substituting $e_0(t) = k_\phi \Omega(t) B_{fm}$ in (15), $B_{fm}$ appears in the loss expression as follows:

$$< P_{t_{op}}(t) >= \frac{1}{k_\phi^2 B_{fm}^2}\frac{1}{T}\int_0^T \frac{A(t)P_{em}^2(t)}{\Omega_m^2(t)}dt + \cdots \quad (16)$$

$$\ldots k_\phi^2 B_{fm}^2\left(\frac{1}{T}\int_0^T\left(B(t) - \frac{\left(X(t)B(t)\right)^2}{A(t)}\right)\Omega_m^2(t)dt\right) + \cdots$$

$$\ldots + \frac{1}{T}\int_0^T \frac{2P_{em}(t)\mathcal{R}_c}{\mathcal{R}_\mu(t)}dt$$

Where $k_\phi$, for the $q$ phases PMSG, can be expressed as:

$$k_\phi = \sqrt{\frac{q}{2}}4n_s\tau_{LR}pr_sR^2 \quad (17)$$

Then, it is possible to find $B_{fm\ opt}$ that minimizes the average losses. It gives:

$$B_{fm\ opt} = \frac{1}{k_\phi}\left(\int_0^T \frac{A(t)P_{em}^2(t)}{\Omega_m^2(t)}dt\right)^{\frac{1}{4}} \times \ldots \quad (18)$$

$$\ldots\left(\frac{1}{\int_0^T\left(B(t) - \frac{\left(X(t)B(t)\right)^2}{A(t)}\right)\Omega_m^2(t)dt}\right)^{\frac{1}{4}}$$

With:

$$< P_{t_{op}} >_{opt} = \frac{2}{T}\sqrt{\int_0^T\left(\frac{\mathcal{R}_c B(t)}{A(t)}\right)\Omega_m^2(t)dt} \times \ldots \quad (19)$$

$$\ldots \frac{2}{T}\sqrt{\int_0^T \frac{A(t)P_{em}^2(t)}{\Omega_m^2(t)}dt} + \frac{1}{T}\int_0^T \frac{2P_{em}(t)\mathcal{R}_c}{\mathcal{R}_\mu(t)}dt$$

Expression (19) depends on $\mathcal{R}_c$, $\mathcal{R}_\mu(t)$ and $X(t)$ which depends on the geometric variables only $(R, r_s, r_w, p)$. Such an expression can be thereby minimized by the use of a genetic algorithm without an excessive computation time.

## IV. MODELING

We consider, in this paper, a 1-D magnetic model. The study is limited at the fundamental components and it is assumed that the steel parts are infinitely permeable.

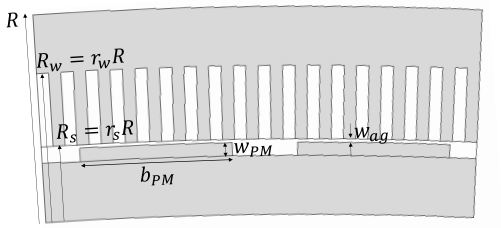


*Fig. 2: Design and geometric parameters of the PMSG*

### A. *Electromagnetic model*

The iron loss resistance $\mathcal{R}_\mu(t)$ can be deduced from the (8). It gives:

$$\mathcal{R}_\mu(t) = \frac{v_{od}^2(t) + v_{oq}^2(t)}{P_{mg}(t)} = \frac{qV_m^2}{2P_{mg}(t)} \quad (20)$$

Where $V_m$ is the magnitude of the voltage which can be expressed from the magnitude of the resulting flux density in the air-gap $B_{rm}$ as below:

$$V_m = 4pn_s\Omega_m RLB_{rm} \quad (21)$$

The iron losses (Eddy currents + hysteresis) can be also expressed as a function of $B_{rm}$ such as [6]:

$$P_{mg}(t) = B_{rm}^2\gamma(t) \quad (22)$$

Where:

$$\gamma(t) = \pi\left(\frac{(1+r_w)r_s^2}{p^2(1-r_w)} + \frac{(r_w^2 - r_s^2)r_s}{k_d r_w}\right)LR^2 \times \ldots \quad (23)$$

$$\ldots k_{ad}(k_{ec}p^2\Omega_m^2(t) + k_h p\Omega_m(t))$$

Thus, from (20)-(23) the iron loss resistance is:

$$\mathcal{R}_\mu(t) = \frac{8}{\pi}qn_s^2\tau_{LR}\frac{1}{k_{ad}(k_{ec}p\Omega_m(t) + k_h)}\ldots \quad (24)$$

$$\ldots\frac{p\Omega_m R}{\left(\frac{1}{k_d}\frac{r_w^2 - r_s^2}{r_w r_s} + \frac{1 - r_w^2}{p^2(1-r_w)^2}\right)}$$

The winding resistance of a nine-phase machine ($\mathcal{R}_c$) can be determined in the same way of a three-phase machine [6]. It can be demonstrated that:

$$\mathcal{R}_c = \frac{16}{\pi} q \left(\frac{k_L}{k_r \sigma_c}\right) n_s^2 \tau_{LR} \frac{p^2}{r_w^2 - r_s^2} \frac{1}{R} \quad (25)$$

The synchronous reactance $X(t)$ of a $q$-phase PMSG can be written:

$$X(t) = \frac{8}{\pi} q \tau_{LR} \mu_0 n_s^2 \frac{r_s R^2}{w_{ag} + w_{PM}} p\Omega_m(t) \quad (26)$$

### B. Constraints

During operation, the hottest point in the machine must remain smaller than the maximum permissible temperature $\theta_{max}$:

$$\theta_w(t) \leq \theta_{max} \quad (27)$$

For each evaluated machine, the dynamic behavior of the temperature in the winding $\theta_w(t)$ is calculated from the lumped parameter thermal model represented in Fig. 3(b) [7] [8]. In this study, the heat flow is assumed unidirectional in the radial direction and each cylindrical element can be modeled by an equivalent circuit as shown in Fig. 3(a). The thermal resistance as well as the thermal capacity are calculated from the geometry and the thermal properties of the materials via (28), (29) and (30). The time-dependent temperature at node $i$ can be evaluated with (31).

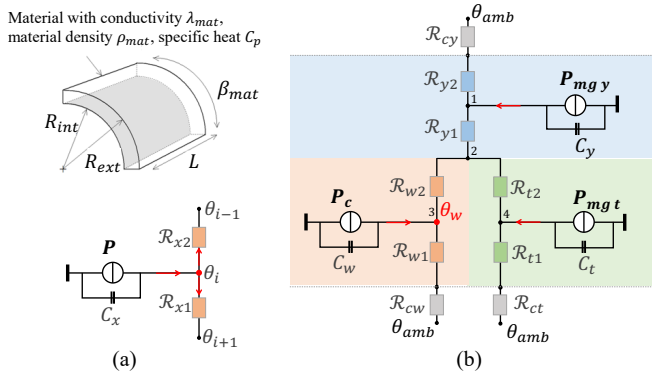


*Fig. 3. (a) Thermal equivalent circuit of a cylindrical element; (b) Lumped parameter thermal model of PMSGs*

$$R_{x1} = \frac{1}{2\lambda_{mat}\beta_{mat}L}\left[\frac{2\left(\frac{R_{ext}}{R_{int}}\right)^2 ln\left(\frac{R_{ext}}{R_{int}}\right)}{\left(\frac{R_{ext}}{R_{int}}\right)^2 - 1} - 1\right] \quad (28)$$

$$R_{x2} = \frac{1}{2\lambda_{mat}\beta_{mat}L}\left[1 - \frac{2ln\left(\frac{R_{ext}}{R_{int}}\right)}{\left(\frac{R_{ext}}{R_{int}}\right)^2 - 1}\right] \quad (29)$$

$$C_x = \frac{1}{2\pi}\rho_{mat} C_p \beta_{mat}(R_{ext}^2 - R_{int}^2)L \quad (30)$$

$$C_x \frac{d\theta_i}{dt} + \frac{\theta_i - \theta_{i-1}}{\mathcal{R}_{x2}} + \frac{\theta_i - \theta_{i+1}}{\mathcal{R}_{x1}} = P \quad (31)$$

Where $P$ is heat generated inside the element. The case of a natural convection at the inner and outer stator surface will be considered here, with a coefficient of 10 W/m²K.

The maximum flux densities in the yoke and teeth must be limited at the saturation level as below:

$$B_{tm}(t) = \frac{1}{k_t} B_{rm} \leq B_{sat} \quad (32)$$

$$B_{ym}(t) = \frac{r_s}{p(1 - r_w)} B_{rm} \leq B_{sat} \quad (33)$$

The terminal voltage is limited at $V_{limit}$ by the power electronics converter and the DC bus voltage. Then:

$$\sqrt{V_d^2 + V_q^2} \leq \sqrt{\frac{q}{2}}\, V_{limit} \quad (34)$$

## V. Application

In this section, the methodology previously presented, will be applied to design a direct-driven PMSG for a 10-MW wind turbine (see specifications given in Tab. 1). A wind speed profile of 4500 points (one point every 10 minutes), measured in the North Sea during one month, will be considered (Fig. 4) [9].

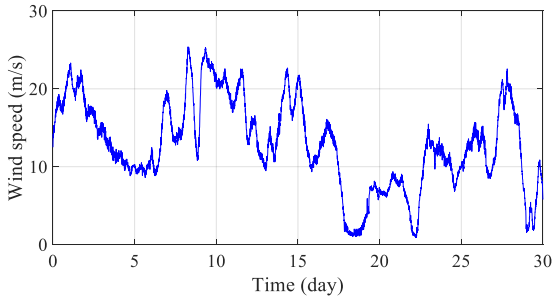


*Fig. 4. Wind speed profile measured at the North Sea in January*

*Tab. 1: Specification of the considered wind turbine*

| | |
|---|---|
| Blade radius, $R_t$ | 82 m |
| Maximal power | 10 MW |
| Cut-in speed | 2.5 m/s |
| Rated speed | 12 m/s |
| Cut-out wind speed | 25 m/s |

The speed and power profiles of the PMSG can be deduced from the wind speed profile and the specifications of the wind turbine, considering the four different operation modes [10] of the wind turbine as represented in Fig. 5.

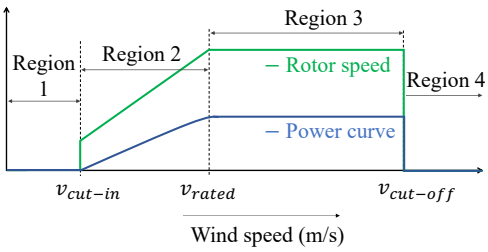


*Fig. 5: Typical power curve and rotor speed of a pitch controlled wind turbine*

In the second region, between $v_{cut-in}$ and the rated speed $v_{rated}$, the maximum power point tracking approach (MPPT) is adopted in order to maximize the captured power [11]. In the third region, the pitch angle is regulated to limit the turbine

output power. The rotor speed and the output power in this region are constants and equal to their rated values. Finally, the speed and torque profiles of the generator can be obtained and presented in Fig. 6.

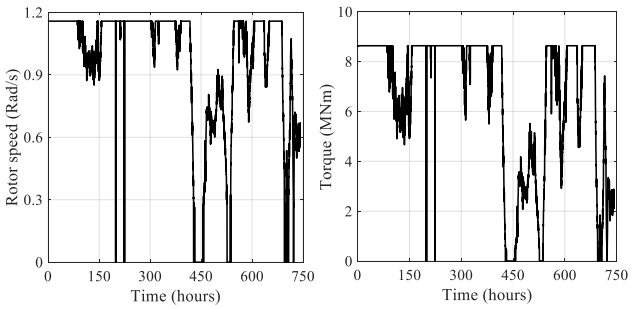


*Fig. 6. Speed-torque profiles for the generator*

### A. Result

The NGSAII algorithm is used to solve the two objective functions:

$$Min\begin{cases} < P_{t_{op}} >_{opt} \\ M_g = M_c + M_{Fe} \end{cases} \quad (35)$$

Where $M_c$ and $M_{Fe}$ are respectively the mass of the copper and the mass of the iron which are calculated as below:

$$M_c = \pi\tau_{LR}(r_w^2 - r_s^2)k_r R^3 \rho_c \quad (36)$$

$$M_{Fe} = \pi\tau_{LR}\left((r_w^2 - r_s^2)k_t + 1 - r_w^2\right)R^3\rho_{Fe} + \cdots \quad (37)$$

$$+\left((2r_s + r_w - 1)R - 2w_{ag} - 2w_{PM}\right) \times \ \ldots$$

$$\times (1 - r_w)\pi\tau_{LR}\, R^2 \rho_{Fe}$$

The main constant parameters used for the optimization are summarized in Tab. 2. The total thickness sum of the air-gap and permanent magnets is chosen equal to 18 mm. The length to outer stator radius ratio is also fixed equal to 0.4. The optimization of these parameters, depending on the power electronics converter, not introduced in this paper, will not be discussed here.

*Tab. 2: Constant parameters*

| Parameter | Value |
|---|---|
| $\tau_{LR}$ | 0.4 |
| $w_{ag} + w_{PM}$ | 18 mm |
| $B_{sat}$ | 2 T |
| $V_{limit}$ | 5 kV |
| $k_{ad}$ | 3 (0.3 mm Si.Fe) |
| $k_{ec}$ | 6.5x10$^{-3}$ (0.3 mm Si.Fe) |
| $k_h$ | 15 (0.3 mm Si.Fe) |
| $h_{eq}$ | 10 W/m²k |
| $\theta_{max}$ | 110°C |
| $\theta_{amb}$ | 20°C |
| $\rho_c$ | 8960 Kg/m$^3$ |
| $\rho_{Fe}$ | 7600 Kg/m$^3$ |
| $\rho_{PM}$ | 7450 Kg/m$^3$ |
| $C_{pc}$ | 390 J/Kg/K |

Considering magnetic and electrical constraints only, the optimization leads to the Pareto-front representing the optimal machines with different maximum permissible temperatures (Fig. 7).

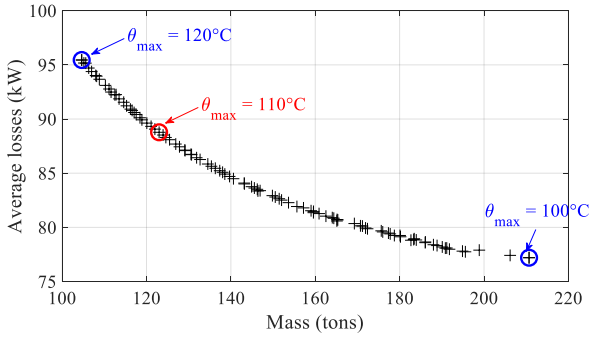


*Fig. 7: Pareto-optimal front of optimal machines*

Tab. 3 summarize the optimal geometry of the optimal generator with a temperature of 110°C. The results are obtained by the use of the thermal constant data presented in Tab. 2. The optimal machine has a weight of 130 tons (including 7 tons of permanent magnets) and consume an average level of losses of 88kW over the considered cycle (leading to an efficiency of 98.5 %). The geometric parameters of the rotor such as thickness and arc of the permanent magnets has been set to obtain the optimal value of $B_{fm\,opt}$. The optimal d-q axis currents versus time are represented in the Fig. 8. It shows that the optimal values of the d-axis component are nonzero leading to a flux weakening mode in most working points.

*Tab. 3: Optimal generator*

| Symbol | Value |
|---|---|
| $R$ | 5.1 m |
| $r_s$ | 0.961 |
| $r_w$ | 0.986 |
| $p$ | 49 |
| $B_{fm}$ | 1 T |
| Mass | 123 tons |
| Average losses | 88 kW |
| $w_{ag}$ | 0.004 m |
| $w_{PM}$ | 0.014 m |
| $b_{PM}$ | 0.252 m |

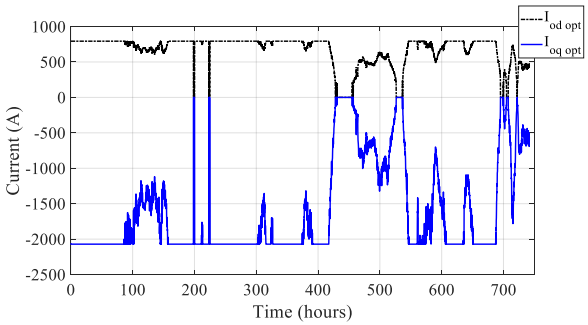


*Fig. 8: Evolution of the optimal d-q axis currents*

Fig. 9 and Fig. 10 show the flux densities and temperature over the cycle for the optimal machine. It shows that the constraints are respected.

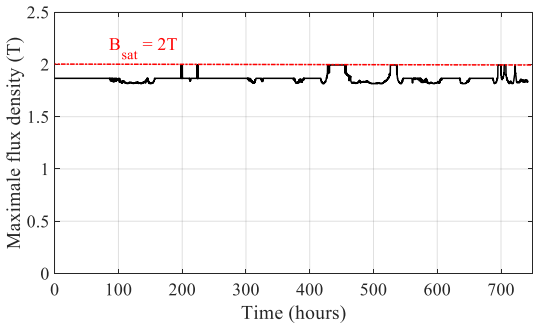


*Fig. 9: Evolution of the maximum flux density in tooth of the optimal generator*

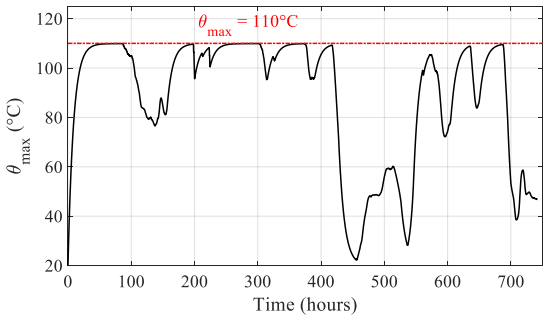


*Fig. 10: Evolution of the temperature in the winding*

### *B. Validation*

In this part, the results for the optimum generator will be validated by a 2D finite element analysis (FEA). Fig. 11 shows the flux lines and the flux density in the machine at the maximum torque with the magnitude of current $I_m = 1.03kA$. The maximum flux density, located in the teeth, is smaller than $B_{sat}$.

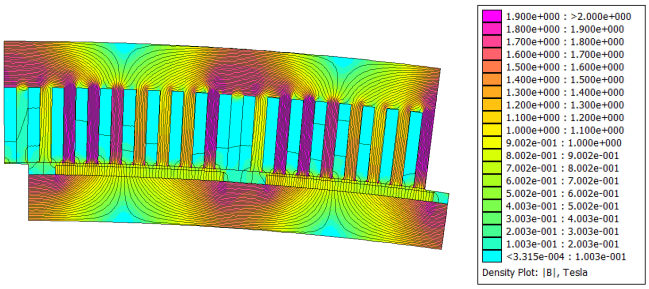


*Fig. 11: Flux lines and flux density at full load*

Fig. 12 represents the torque as a function of the current and Fig. 13 the waveform of the EMF. The results obtained with the FEA validate the analytical model used (see Tab. 4).

*Tab. 4: Maximum torque and EMF at 10 MW- 11rpm.*

| | Analytical model | FEA | Variation |
|---|---|---|---|
| Torque (MNm) | 8.6 | 8.2 | 5% |
| Magnitude of the EMF (1st harmonic) (kV) | 2.31 | 2.29 | 1% |

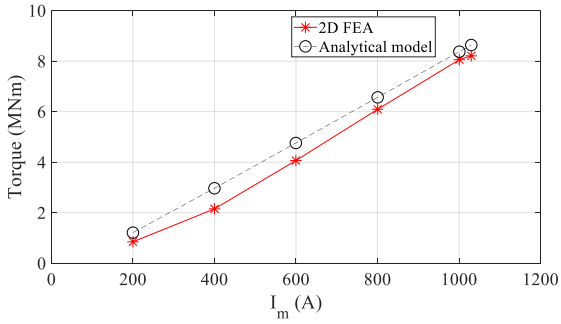


*Fig. 12: Variation of the torque versus current*

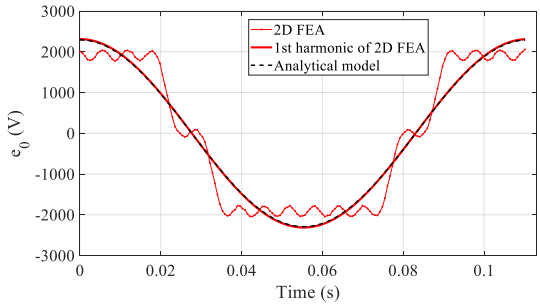


*Fig. 13: EMF at 10 MW- 11rpm*

In order to validate the thermal model, the evolution of the temperature in the winding has been calculated considering a step of power (see Fig. 14) with copper and iron losses in the yoke and tooth at full load, for $I_{d_{opt}}$= 771A and $I_{q_{opt}}$= -2 kA. The result (Tab.5) show that both the transient and the final temperature in the winding are in a good agreement.

*Tab. 5: Losses of the optimal generator at the maximal power (10MW, 1.03kA)*

| | Analytical model | FEA | Variation |
|---|---|---|---|
| Iron losses in the yoke | 22 kW | 30 kW | -36% |
| Iron losses in the teeth | 32 kW | 23 kW | 28% |
| Total iron of the stator | 54 kW | 53kW | 2% |
| Copper losses | 62 kW | | |

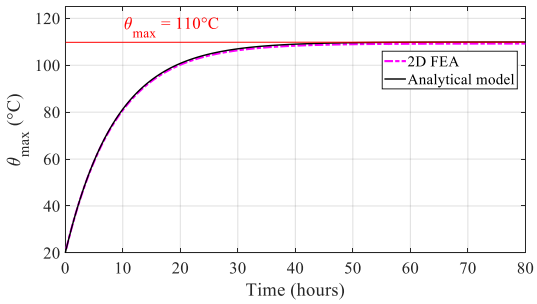


*Fig. 14: Evolution of the temperature in the winding at the maximal power*

## VI. CONCLUSION

This paper has presented a general method allowing to design a PMSG from the torque and speed profiles made of several thousand working points. As shown in the paper, the optimization of the PMSG, with 4500 working points, has been successfully done in a few minutes. The 1-D model used has been validated by a 2D finite element analysis. As it was shown, the method allows to optimize the control parameters

(via $I_{od}(t)$ and $I_{oq}(t)$) leading to optimize the flux weakening. The dynamic thermal behavior is also controlled, avoiding an oversizing of the machine in the case the permanent thermal regime is not reached. Finally, this approach with its quickness and simplicity, constitutes a first step toward a design optimization of the complete turbine system, including the power electronics components which will be discussed in future works.

## VII. REFERENCES


[1] Z. Q. Zhu and J. Hu, "Electrical machines and power-electronic systems for high-power wind energy generation applications : Part I - market penetration , current technology and advanced machine systems," *COMPEL Int. J. Comput. Math. Electr. Electron. Eng. Emerald Artic.*, no. December, 2012.

[2] C. Stuebig, A. Seibel, K. Schleicher, L. Haberjan, and M. Kloepzig, "Electromagnetic Design of a 10 MW Permanent Magnet Synchronous Generator for Wind Turbine Application," in *IEEE International Electric Machines & Drives Conference (IEMDC)*, 2015, pp. 1202–1208.

[3] J. Wang *et al.*, "Design of a Superconducting Synchronous Generator With LTS Field Windings for 12 MW Offshore Direct-Drive Wind Turbines," *IEEE Trans. Ind. Electron.*, vol. 63, no. 3, pp. 1618–1628, 2016.

[4] P. Lazari, S. Member, J. Wang, S. Member, and L. Chen, "A Computationally Efficient Design Technique for Electric-Vehicle Traction Machines," *IEEE Trans. Ind. Appl.*, vol. 50, no. 5, pp. 3203–3213, 2014.

[5] L. Dang, N. Bernard, N. Bracikowski, and G. Berthiau, "Design Optimization with Flux Weakening of High-Speed PMSM for Electrical Vehicle Considering the Driving Cycle," *IEEE Trans. Ind. Electron.*, vol. 64, no. 12, pp. 9834–9843, 2017.

[6] N. Bernard, R. Missoum, L. Dang, N. Bekka, H. Ben Ahmed, and M. E. Za, "Design Methodology for High-Speed Permanent Magnet Synchronous Machines," vol. 31, no. 2, pp. 477–485, 2016.

[7] P. H. Mellor, D. Roberts, and D. R. Turner, "Lumped parameter thermal model for electrical machines of TEFC design," in *IEE Proc. B - Electric Power Applications*, 1991, vol. 138, no. 5.

[8] N. Bernard, H. Ben Ahmed, B. Multon, C. Kerzreho, J. Delamare, and F. Faure, "Flywheel energy storage systems in hybrid and distributed electricity generation," in *in PCIM 2003, Nuremberg, 22-24 may*, 2003.

[9] "https://vortexfdc.com/." .

[10] V. Sohoni, S. C. Gupta, and R. K. Nema, "A Critical Review on Wind Turbine Power Curve Modelling Techniques and Their Applications in Wind Based Energy Systems," *J. Energy*, pp. 1–18, 2016.

[11] K. Kim, T. L. Van, S. Member, D. Lee, S. Song, and E. Kim, "Maximum Output Power Tracking Control in Variable-Speed Wind Turbine Systems Considering Rotor Inertial Power," *IEEE Trans. Ind. Electron.*, vol. 60, no. 8, pp. 3207–3217, 2013.